Localized modes in defect-free two-dimensional circular photonic crystals

Wei Zhong and Xiangdong Zhang*

Department of Physics, Beijing Normal University, Beijing 100875, People's Republic of China

(Received 19 July 2009; revised manuscript received 13 September 2009; published 6 January 2010)

The localization of electromagnetic waves in defect-free circular photonic crystals (CPCs) is investigated using a multiple-scattering method. It is shown that electromagnetic waves of certain freqencies are localized in some special regions inside a perfect CPC with a high order of rotational symmetry. Localized modes with a high Q factor, greater than 10^6, are obtained. In particular, some unique localized modes such as circular modes and localized modes for both polarized waves are found in the present system, which are completely different from those in defect-free photonic quasicrystals and periodic structures. Their physical properties are also analyzed.

DOI: 10.1103/PhysRevA.81.013805 PACS number(s): 42.70.Qs, 42.60.Da, 41.20.Jb

I. INTRODUCTION

Photonic crystals (PCs) have been intensively studied both theoretically and experimentally during the past two decades [1–3]. Since PCs can have spectral gaps in which electromagnetic wave propagation is forbidden in all directions, they offer the possibility of controlling the flow of photons in a manner analogous to that for electrons in a semiconductor [4–8]. For example, if some defects are introduced by locally breaking the spatial periodicity in PCs, the defect modes or cavity modes can be found for frequencies in the band gaps [9–11]. These localized modes can be used to develop new types of lasers, design various waveguides, and provide other related applications in optoelectronics [12–15].

In fact, band gaps exist not only in periodic PCs but also in some photonic quasiperiodic structures [16–19]. The same method for and concept of the defect states in periodic PCs can be applied to photonic quasicrystals (QCs) [20]. If no defect is present, the structure is called "defect-free." In contrast to periodic PCs, photonic QCs possess some special properties which can occur in localized states in some defect-free systems [21–23]. However, these defect-free localized modes are only for a certain polarized wave, the S wave (TM polarization) or P wave (TE polarization). The localized mode for all polarized waves has not been observed in these defect-free systems so far.

Recently, another type of nonperiodic photonic structure, that is, the circular photonic crystal (CPC), was brought to our attention [24–28]. The lattice arrangement of the CPC is the same as that of ring structures in microstructured optical fibers [29,30]. The CPC possesses $2\pi/n$ rotational symmetry, where n is the rotational fold number. It has been shown that isotropic photonic gaps exist in the CPC [24]. Based on the CPC, a high-Q-factor microcavity and a transmission waveguide with a low radius of curvature at a bend can be easily realized [24–28]. In this work, we investigate localized properties of electromagnetic waves in defect-free CPC structures. Some unique localized modes, such as circular modes and localized modes for both polarized waves, are found in these systems. Their physical properties are also analyzed. The rest of the paper is arranged as follows. In Sec. II, we define the system and introduce the method of numerical simulation. The results and discussion are presented in Sec. III. The conclusion is given in Sec. IV.

II. SYSTEM AND METHOD

We consider a CPC consisting of dielectric cylinders embedded in an air background. The positions of the dielectric cylinders in the xy plane for an n-fold symmetric structure are given by [24]

$$x = aN\cos\left(\frac{2m\pi}{nN}\right), \qquad y = aN\sin\left(\frac{2m\pi}{nN}\right), \tag{1}$$

where N represents the number of concentric circles (with the number of rods being 1 for $N = 0$), a is the difference of radii in neighboring concentric circles, and m represents the mth cylinder in the Nth concentric cycle ($0 \leqslant m \leqslant nN$). This type of CPC can exhibit arbitrary-order rotational symmetry. A 10-fold sample with $N = 5$ is shown in Fig. 1 as an example. In the following, we study the gap structures and localized properties of electromagnetic waves in CPCs with various rotational symmetries using the multiple-scattering method.

The multiple-scattering method is best suited for a finite collection of cylinders with a continuous incident wave of fixed frequency. For circular cylinders, the scattering property of the individual cylinder can be obtained analytically, relating the scattered fields to the incident fields. The total field, which includes the incident plus the multiple-scattered field, can then be obtained by solving a linear system of equatwhose size is proportional to the number of cylinders in the system. Both near-field and far-field radiation patterns can be obtained straightforwardly.

To obtain the band-gap information for a CPC, we calculate the total energy flow of the system, which is excited by a point light source at a fixed frequency located near the center of the sample (see Fig. 1). The Poynting vector of the radiated field at position $\vec{r}$, $\vec{S}(\vec{r})$, can be calculated by the multiple-scattering method, from which the total radiation power P_s

*zhangx@bnu.edu.cn

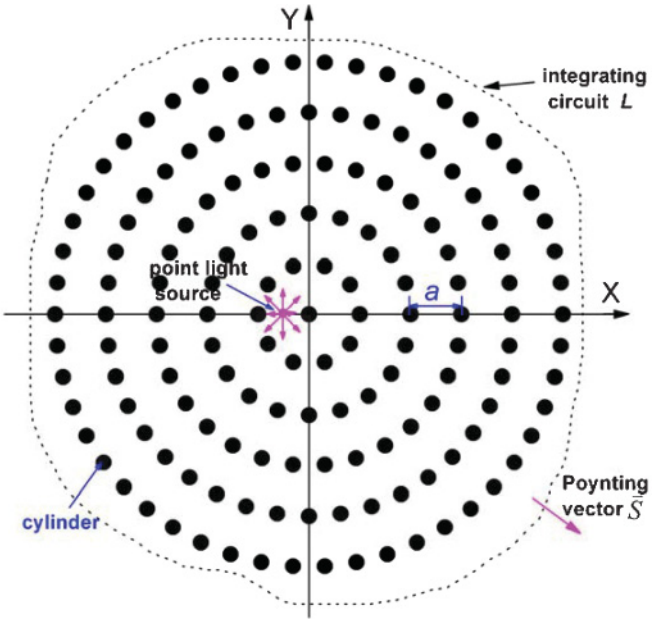

FIG. 1. (Color online) Scheme of a 10-fold CPC lattice structure and setup for calculation of the total radiation energy flow.

can be expressed as

$$P_s = \oint_L \vec{S}(\vec{r}) \cdot \vec{\tau} d\vec{r}, \tag{2}$$

where L represents a close path outside the CPC and $\vec{\tau}$ is a unit vector perpendicular to the integrating line L. Since the spectrum of P_s includes transmission from all directions, it can be used to determine the position of a complete photonic gap. For frequencies inside a full gap, the density of state is zero, which in turn gives a divergent input impedance and vanishing P_s. Therefore, a gap in the spectrum of P_s represents the existence of a complete photonic gap in the system. The validity of this method was demonstrated in our previous investigation [18].

In addition, we can obtain some information on localized states from the spectrum of the radiation power. In general, if localized states exist in the gap, sharp peaks can be observed in the spectrum. Then, combining the calculation of the local density of states (LDOS) and the eigenfield, we can investigate the properties of these localized states. For a finite structure, the LDOS is given by the imaginary part of the electric Green's tensor $G^e(\vec{r}, \vec{r}_s; \omega)$ [31]:

$$\rho(\vec{r}; \omega) = -\frac{2\omega\varepsilon}{\pi c^2} \mathrm{Im}[G^e(\vec{r}, \vec{r}; \omega)]. \tag{3}$$

Here $G^e(\vec{r}, \vec{r}_s; \omega)$ is the electric Green's function for a source at $\vec{r}_s$ and observation point at $\vec{r}$, ω is the frequency, and c is the velocity of the light in vacuum. The Green's function in the CPC can also be calculated by using the multiple-scattering method [31]. Thus, the LDOS can be obtained exactly.

III. NUMERICAL RESULTS AND DISCUSSION

In this section, we provide the calculated results for localized properties of electromagnetic waves in defect-free CPCs with different orders of rotational symmetry. The

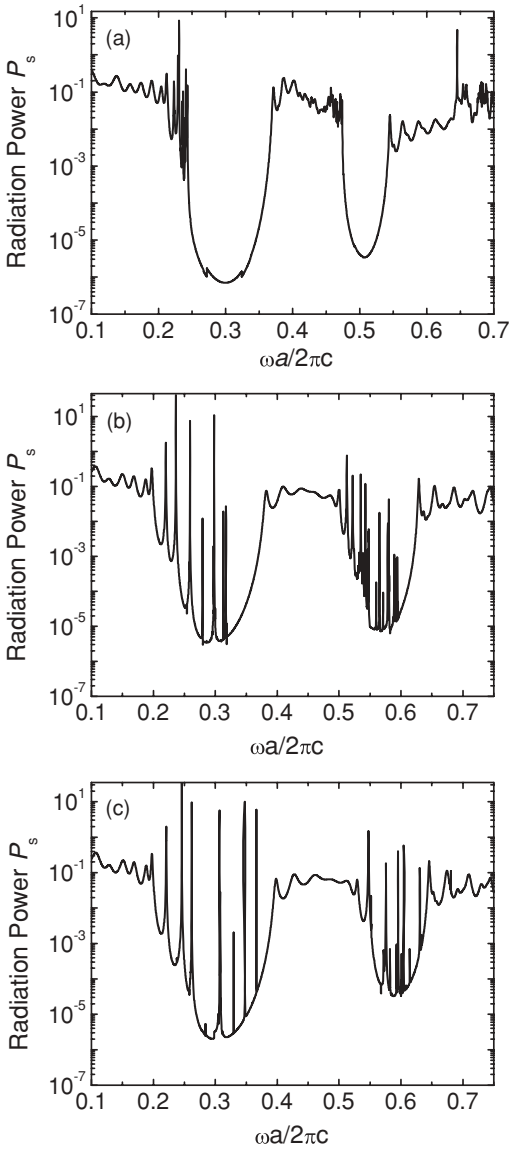

FIG. 2. Radiation powers for various CPC structures. The point source is located at $x = -0.5a$ and $y = 0.0$. The dielectric constant of the cylinder is taken as 11.4. (a) Sixfold CPC with radius $R = 0.25a$ and number of concentric circles $N = 6$; (b) 10-fold CPC with $R = 0.22a$ and $N = 5$; (c) 12-fold CPC with $R = 0.20a$ and $N = 5$.

calculated results of the radiation power for 6-, 10-, and 12-fold CPCs are plotted in Figs. 2(a)–2(c), respectively. Here only the TM polarization is considered and the dielectric constant ε of the cylinder is taken as 11.4. The radius R of the cylinder is taken as $0.2a$ for 12-fold, $0.22a$ for 10-fold, and $0.25a$ for 6-fold CPCs. The number of concentric circles N is taken as 5 for 12-fold and 10-fold, and as 6 for 6-fold, CPCs. The point source is arranged at $x = -0.5a$ and $y = 0.0$. The spectra of the radiation power show clearly that band gaps exist in all structures. For the sixfold CPC, defect-free localized states are found in the band regions [27]. However, the spectrum is smooth inside the gaps. In contrast, some sharp peaks (defect states) appear within the gaps for the 10- and 12-fold CPCs. For example, there are seven sharp peaks in the first gap of the

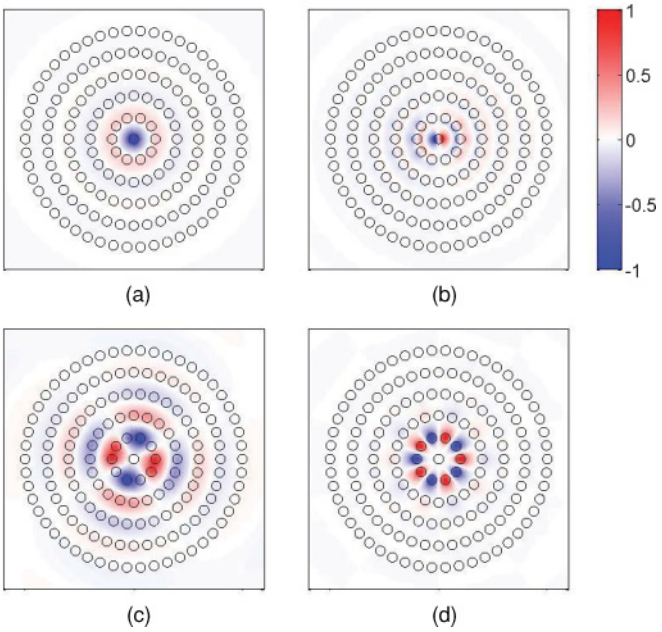

FIG. 3. (Color online) Distributions of the electric field in a 10-fold CPC at different frequencies, (a) $\omega a/2\pi c = 0.2363$, $Q = 6.95 \times 10^3$, (b) $\omega a/2\pi c = 0.5125$, $Q = 1.43 \times 10^3$, (c) $\omega a/2\pi c = 0.2201$, $Q = 640$, and (d) $\omega a/2\pi c = 0.3171$, $Q = 3.22 \times 10^5$, which correspond to the peaks in the low-transmission regions in Fig. 2(b).

10-fold CPC, and more in the second gap. These defect states were not caused by any physical defects within the structure but occurred because the order of the rotational symmetry was changed. At the same time, they also depend on the size of the sample and the dielectric constant of the cylinder. If the size of the sample is increased, the quantities of localized states increase. In the following, we focus our discussion on these localized states.

To study these localized states in a more detailed manner, an eigenvalue analysis is required. The distributions of the eigenfield at the frequencies corresponding to the peaks in the low-transmission regions in Fig. 2 were calculated. The results show that localizations of the electromagnetic wave have indeed taken place. Different types of localized modes have been observed. For example, the distributions of the electric field in a 10-fold CPC at several frequencies are plotted in Figs. 3(a)–3(d). The modes at $\omega a/2\pi c = 0.2363$, 0.5125, and 0.2201 possess monopole, dipole, and quadrupole radiation patterns, respectively, whereas there is 10-fold symmetry at $\omega a/2\pi c = 0.3171$. These localized modes resemble spherical harmonic functions that depend on the frequency and order of the rotational symmetry of the CPC. This is similar to the data for localized modes in photonic QCs, and their physical origins are also the same. The superiority of the present system is that modes with a high Q value can be found via the isotropic confinement effect. For example, at $\omega a/2\pi c = 0.3171$ the Q factor can reach 3.217×10^5, although a resonant cavity does not exist. According to a previous investigation [32], here the Q factor for the localized state is defined as $\lambda/\Delta\lambda$ (where λ is the wavelength and $\Delta\lambda$ represents the half-width of the peak).

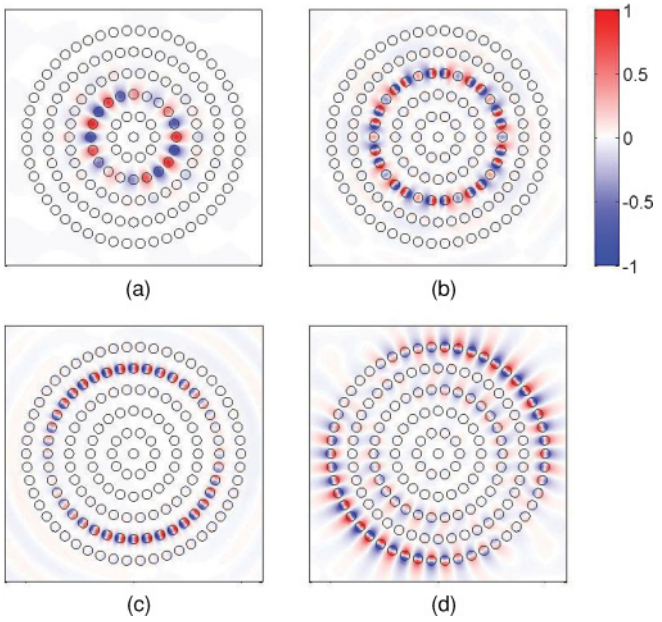

FIG. 4. (Color online) Distributions of the electric field in a 10-fold CPC at different frequencies, (a) $\omega a/2\pi c = 0.3128$, $Q = 1.51 \times 10^5$, (b) $\omega a/2\pi c = 0.5599$, $Q = 4.34 \times 10^3$, (c) $\omega a/2\pi c = 0.5952$, $Q = 8.88 \times 10^3$, and (d) $\omega a/2\pi c = 0.5325$, $Q = 2.66 \times 10^3$, which correspond to the peaks in the low-transmission regions in Fig. 2(b).

The unique feature of the present system is that the electromagnetic waves can be localized along various circular layers. Figure 4 displays this feature. Figures 4(a)–4(d) describe the distribution of the electric field in a 10-fold CPC at

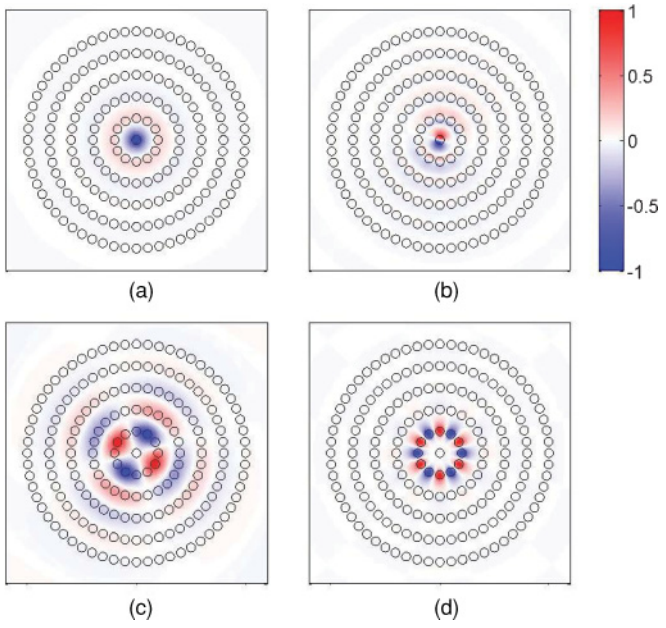

FIG. 5. (Color online) Distributions of the electric field in a 12-fold CPC at different frequencies, (a) $\omega a/2\pi c = 0.2459$, $Q = 1.52 \times 10^4$, (b) $\omega a/2\pi c = 0.5475$, $Q = 1.41 \times 10^3$, (c) $\omega a/2\pi c = 0.2207$, $Q = 9.46 \times 10^2$, and (d) $\omega a/2\pi c = 0.3666$, $Q = 1.32 \times 10^6$, which correspond to the peaks in the low-transmission regions in Fig. 2(c).

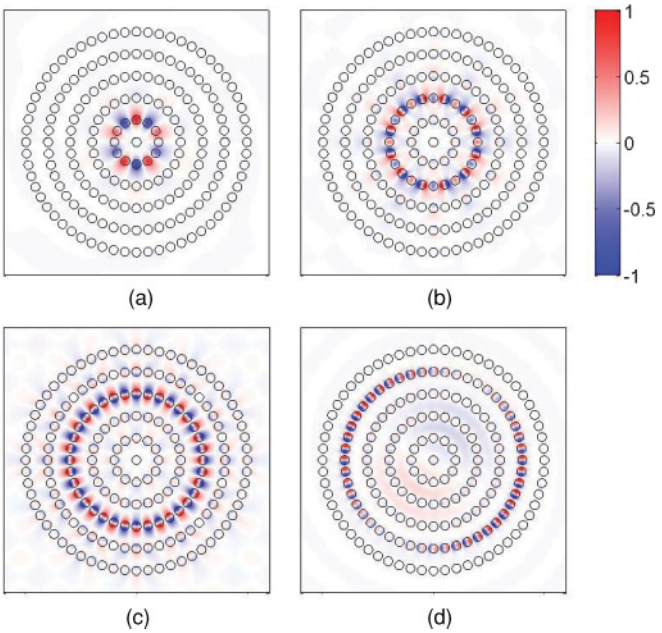

FIG. 6. (Color online) Distributions of the electric field in a 12-fold CPC at different frequencies, (a) $\omega a/2\pi c = 0.3478$, $Q = 5.05 \times 10^5$, (b) $\omega a/2\pi c = 0.5936$, $Q = 1.60 \times 10^4$, (c) $\omega a/2\pi c = 0.6009$, $Q = 7.78 \times 10^3$, and (d) $\omega a/2\pi c = 0.6807$, $Q = 6.95 \times 10^3$, which correspond to the peaks in the low-transmission regions in Fig. 2(c).

$\omega a/2\pi c = 0.3128$, 0.5599, 0.5952, and 0.5325 [corresponding to some of the sharp peaks in Fig. 2(b)], respectively. The circular localized modes in the different circular layers are shown clearly. Such localized modes cannot be found in

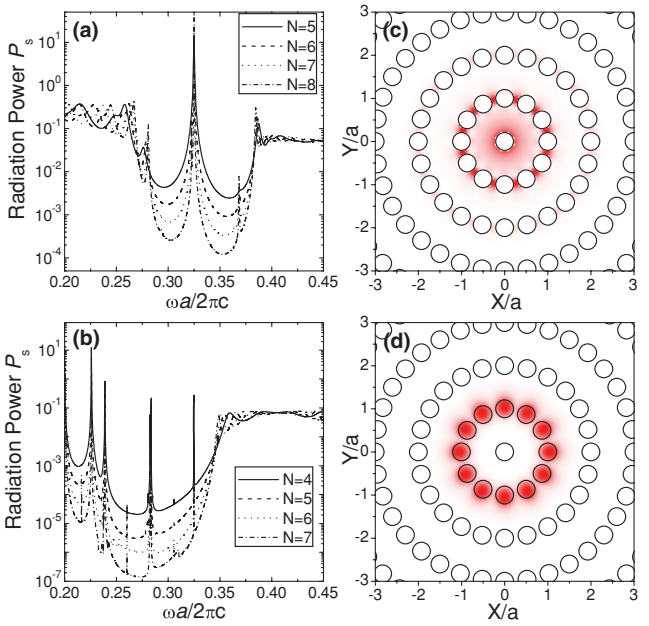

FIG. 7. (Color online) (a, b) Radiation powers for 12-fold CPC structures of various sample sizes at $\varepsilon = 11.4$ and $R = 0.231a$ for the TE and TM modes, respectively. The point source is located at $x = -0.5a$ and $y = 0.0$. (c, d) Distributions of the LDOS at $\omega a/2\pi c = 0.3249$ for TE and TM polarization, respectively. The LDOS map is in linear false-color scale [red (dark), high; white, low].

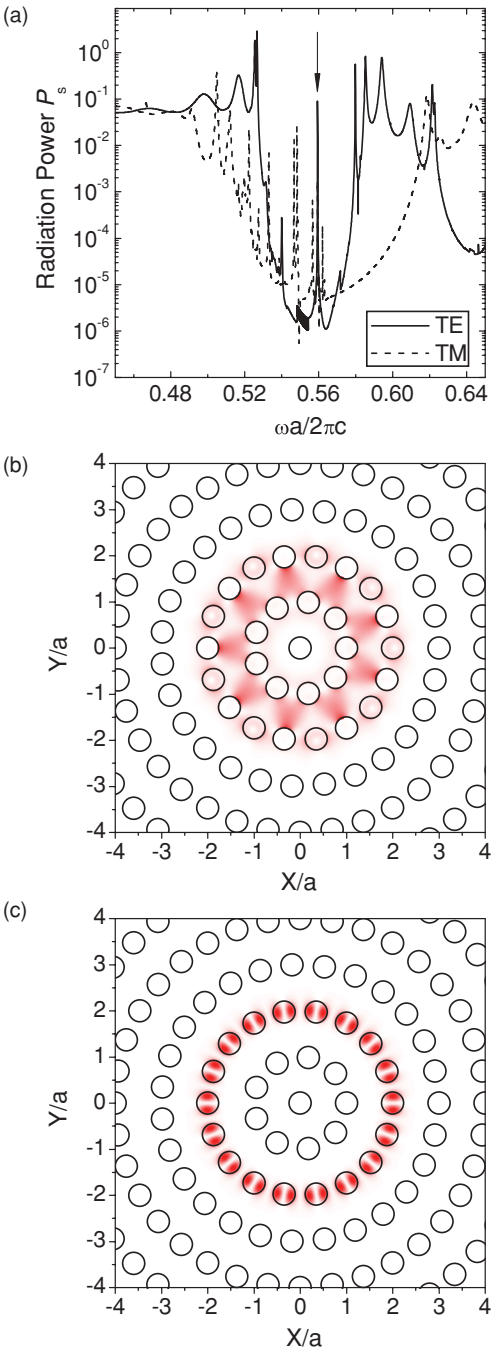

FIG. 8. (Color online) Absolute localized modes in a ninefold CPC with $\varepsilon = 11.4$, $R = 0.226a$, and $N = 5$. (a) Radiation powers for TE (solid line) and TM (dashed line) polarization. (b) Distribution of the LDOS for TE polarization at $\omega a/2\pi c = 0.5594$. The LDOS map is in linear false-color scale [red (dark), high; white, low]. (c) The corresponding distribution of the LDOS for TM polarization at the same frequency.

defect-free photonic QCs or periodic structures, which are determined by the special property of the CPC structure.

In fact, these unique properties not only exist in the 10-fold CPC but also can be found in other CPC structures with different orders of rotational symmetry, such as 9-, 11-, 12-, 13-, and 14-fold structures. For example, some localized modes in a 12-fold CPC are plotted in Figs. 5 and 6.

Figures 5(a)–5(d) represent the distribution of the electric field at $\omega a/2\pi c = 0.2459, 0.5475, 0.2207$, and 0.3666 [corresponding to some of the sharp peaks in Fig. 2(c)], respectively. The results are similar to those for the 10-fold CPC in Fig. 3. However, localized modes which possess a higher Q value can be demonstrated. For example, the Q factor can reach $Q = 1.301 \times 10^6$ at $\omega a/2\pi c = 0.3666$.

We also found that the localized modes with the highest Q values correspond to the rotational symmetry of the structure. For example, the localized modes with the highest Q values in 9-, 10-, 11-, 12-, 13-, and 14-fold CPC structures are those possessing 9-, 10-, 11-, 12-, 13-, and 14-fold symmetries, respectively. In addition, circular localized modes in different circular layers can be observed, as shown in Fig. 6, which are also similar to Fig. 4 for the 10-fold CPC. This means that a bent waveguide can be designed by use of a CPC without any defect that allows high transmission with any radius of curvature at a bend.

The preceding discussion has focused on only one kind of polarized mode, the TM localized mode. In fact, similar phenomena can also be observed for the TE polarized mode. It is interesting that the localized mode for both polarized waves in CPC structures can be observed by tuning the parameters of the cylinder. Figures 7(a) and 7(b) display the radiation power as a function of the frequency for 12-fold CPCs of different sample sizes at $\varepsilon = 11.4$ and $R = 0.231a$ for TE and TM polarized waves, respectively. The sample size is depicted by the number of concentric-circle layers N. It is shown clearly that the dips increase in depth with the sample size for some frequency regions, $\omega a/2\pi c = 0.283$ to 0.381 for the TE mode and $\omega a/2\pi c = 0.2$ to 0.345 for the TM mode. This exhibits the gap feature, which is in contrast to the band region. In band regions, radiation powers or transmission coefficients do not decrease with an increase in sample size. This means that the resonant peaks in these regions actually represent the defect states within the gap region.

Among these defect states, we find that two resonant peaks for TM and TE polarizations overlap at $\omega a/2\pi c = 0.3249$. The corresponding distributions of the LDOS for TM and TE polarizations at this frequency are plotted in Figs. 7(c) and 7(d), respectively. The localizations of the electromagnetic wave around the same region at the same frequency are demonstrated. This means that both polarized waves at $\omega a/2\pi c = 0.3249$ can be confined in the sample at the same time. This phenomenon can also be realized in a ninefold CPC if we choose a cylinder with $R = 0.226a$ to construct the sample. The solid line and dashed line in Fig. 8(a) represent the radiation powers for the TE and TM polarized modes in a ninefold CPC with $N = 5$, respectively. Two resonant peaks for TE and TM polarizations overlap at $\omega a/2\pi c = 0.5594$, as marked by the arrow. The corresponding distributions of the LDOS for TE and TM polarizations are plotted in Figs. 8(b) and 8(c), respectively. The localizations of the electromagnetic wave around the same region at the same frequency are again observed.

IV. CONCLUSION

Based on the multiple-scattering method, we have investigated the localizations of electromagnetic waves in defect-free CPC structures. The radiation power, LDOS, and eigenfield in these systems have been calculated. We have found that electromagnetic waves of certain frequencies can be localized to some special regions inside the perfect CPC with high orders of rotational symmetry. Not only have some localized modes with a high Q factor, greater than 10^6, been obtained, but also circular modes and localized modes for both polarized waves have been found in the present structures. These localized modes are unique, being determined by the circular structure of the CPC, and cannot be found in defect-free photonic QCs and other periodic structures. We believe that our findings can provide important references for developing new types of lasers and designing waveguides with high transmission and any radius of curvature at a bend.

ACKNOWLEDGMENTS

This work was supported by the National Natural Science Foundation of China under Grant No. 10825416 and the National Key Basic Research Special Foundation of China under Grant No. 2007CB613205.

[1] J. D. Joannopoulos, R. D. Meade, and J. N. Winn, *Photonic Crystal—Molding the Flow of Light* (Princeton University Press, Princeton, NJ, 1995).
[2] C. M. Soukoulis, ed., *Photonic Band Gap Materials* (Kluwer Academic, Dordrecht, 1996).
[3] K. Sakoda, *Optical Properties of Photonic Crystals* (Springer, New York, 2001).
[4] E. Yablonovitch, Phys. Rev. Lett. **58**, 2059 (1987).
[5] S. John, Phys. Rev. Lett. **58**, 2486 (1987).
[6] K. M. Ho, C. T. Chan, and C. M. Soukoulis, Phys. Rev. Lett. **65**, 3152 (1990).
[7] K. M. Leung and Y. F. Liu, Phys. Rev. Lett. **65**, 2646 (1990).
[8] Z. Zhang and S. Satpathy, Phys. Rev. Lett. **65**, 2650 (1990).
[9] E. Yablonovitch, T. J. Gmitter, R. D. Meade, A. M. Rappe, K. D. Bommer, and J. D. Joannopoulos, Phys. Rev. Lett. **67**, 3380 (1991).
[10] M. Sigalas, C. M. Soukoulis, E. N. Economou, C. T. Chan, and K. M. Ho, Phys. Rev. B **48**, 14121 (1993).
[11] A. R. McGurn, Phys. Rev. B **53**, 7059 (1996).
[12] O. Painter, R. K. Lee, A. Scherer, A. Yariv, J. D. OBrien, P. D. Dapkus, and I. Kim, Science **284**, 1819 (1999).
[13] A. Mekis, J. C. Chen, I. Kurland, S. Fan, P. R. Villeneuve, and J. D. Joannopoulos, Phys. Rev. Lett. **77**, 3787 (1996).
[14] K. C. Kwan, X. Zhang, Z. Q. Zhang, and C. T. Chan, Appl. Phys. Lett. **82**, 4414 (2003).
[15] J. D. Joannopoulos, P. R. Villeneuve, and S. Fan, Nature (London) **386**, 143 (1997).

[16] Y. S. Chan, C. T. Chan, and Z. Y. Liu, Phys. Rev. Lett. **80**, 956 (1998).
[17] M. E. Zoorob, M. D. B. Chartton, G. J. Parker, J. J. Baumberg, and M. C. Netti, Nature (London) **404**, 740 (2000).
[18] X. Zhang, Z. Q. Zhang, and C. T. Chan, Phys. Rev. B **63**, 081105(R) (2001).
[19] A. Della Villa, S. Enoch, G. Tayeb, V. Pierro, V. Galdi, and F. Capolino, Phys. Rev. Lett. **94**, 183903 (2005).
[20] S. S. M. Cheng, L. M. Li, C. T. Chan, and Z. Q. Zhang, Phys. Rev. B **59**, 4091 (1999).
[21] Y. Wang, X. Hu, X. Xu, B. Cheng, and D. Zhang, Phys. Rev. B **68**, 165106 (2003).
[22] A. Della Villa, S. Enoch, G. Tayeb, F. Capolino, V. Pierro, and V. Galdi, Opt. Express **14**, 10021 (2006).
[23] K. Mnaymneh and R. C. Gauthier, Opt. Express **15**, 5089 (2007).
[24] N. Horiuchi, Y. Segawa, T. Nozokido, K. Mizumo, and H. Miyazaki, Opt. Lett. **29**, 1084 (2004); **30**, 973 (2005).
[25] J. Scheuer and A. Yariv, Phys. Rev. E **70**, 036603 (2004); D. Chang, J. Scheuer, and A. Yariv, Opt. Express **13**, 9272 (2005).
[26] J. Chaloupka, J. Zarbakhsh, and K. Hingerl, Phys. Rev. B **72**, 085122 (2005).
[27] S. Xiao and M. Qiu, Photon. Nanostruct. Fundam. Appl. **3**, 134 (2005); Phys. Lett. **A340**, 474 (2005).
[28] P.-T. Lee, T.-W. Lu, J.-H. Fan, and F.-M. Tsai, Appl. Phys. Lett. **90**, 151125 (2007).
[29] J. Xu, J. Song, C. Li, and K. Ueda, Opt. Commun. **182**, 343 (2000).
[30] M. A. van Eijkelenborg, M. C. J. Large, A. Argyros, J. Zagari, S. Manos, N. A. Issa, I. Bassett, S. Fleming, R. C. McPhedran, C. M. de Sterke, and N. A. P. Nicorovici, Opt. Express **9**, 319 (2001).
[31] A. A. Asatryan, K. Busch, R. C. McPhedran, L. C. Botten, C. M. de Streke, and N. A. Nicorovici, Phys. Rev. E **63**, 046612 (2001); Opt. Express **8**, 191 (2001).
[32] J. S. Foresi, P. R. Villeneuve, J. Ferrera, E. R. Thoen, G. Steinmeyer, S. Fan, J. D. Joannopoulos, L. C. Kimerling, H. I. Smith, and E. P. Ippen, Nature (London) **390**, 143 (1997).